Journal of Inorganic and Organometallic Polymers and Materials
https://doi.org/10.1007/s10904-025-03591-0

BRIEF REPORT

Magnetic Composite Nanofibers as Advanced Adsorbents for Toluidine Blue and Congo Red Dyes

Hajer Tlili[1,2] · Anis Elaoud[2,3] · Nedra Asses[2] · Jesús A. Fuentes-García[4,5] · Karima Horchani-Naifer[1] · Mounir Ferhi[1]

Received: 27 August 2024 / Accepted: 1 January 2025

Abstract

This study introduces an innovative method to remove dyes using a composite material of magnetite nanoparticles (MNPs) immobilized in nanofibers (MNFs). Produced via a simple electrospinning method, the MNFs exhibited excellent adsorptive properties, including a uniform average diameter of 0.3 ± 0.06 µm, a BET surface area of 9.9457 ± 0.0363 m^2 g^{-1}, a pore volume of 0.02 cm^3 g^{-1}, and a pore size of 8.778 nm. Chemical and thermal analyses confirmed the composite's characteristics. The adsorption performance of MNFs was assessed using two ionic dyes: cationic Toluidine Blue (TB) and anionic Congo Red (CR). Compared to MNPs, MNFs achieved significantly higher adsorption capacities, with values of 325 mg g^{-1} for TB and 350 mg g^{-1} for CR at a dye concentration of 1 g L^{-1}. The adsorption kinetics were analyzed, fitting well with the Pseudo-Second-Order model. The MNFs demonstrated enhanced adsorption capacities, increasing by up to 15% for TB and 20% for CR compared to MNPs under identical conditions. These results underscore MNFs' potential as effective adsorbents for dye removal, offering an environmentally friendly and cost-effective treatment for industrial wastewater.

Keywords Inorganic reinforcement · Polymer matrix · Adsorption kinetics · Ionic dyes · Water pollution

1 Introduction

The pollution of natural and artificial water bodies is one of the most serious environmental issues caused by industrial development and rapid population growth. This problem has worsened over time and has become a global concern due to the large volume of wastewater discharged into basins, rivers, and seas, which affects aquatic biodiversity. Printing and dyeing wastewater is among the most hazardous types of water pollution, capable of altering water color and properties even at very low concentrations. This kind of wastewater is typically produced in various industries, including textiles, cosmetics, tanning, photography, food, and plastics. It is estimated that the annual production of dyes amounts to approximately 1.6 million tons, of which 10–15% is released into the environment as wastewater [1].

In this context, the textile industry, which depends heavily on water for its processes, is identified as the main contributor to dyeing wastewater, with an estimated annual discharge of 200 million liters [2]. The release of dye molecules into water bodies through effluents poses serious threats to aquatic life. Changes in water quality, such as contamination by heavy metals and aromatic compounds,

✉ Mounir Ferhi
ferhi.mounir@gmail.com

1 Laboratory of Physico-Chemistry of Mineral Materials and Their Applications, National Center for Research in Materials Sciences CNRSM, Technopole Borj Cedria, BP. 73, 8027 Soliman, Tunisia

2 Laboratory of Environmental Sciences and Technologies, Higher Institute of Environmental Sciences and Technologies, University of Carthage, BP 1003, 2050 Hammam Lif, Tunisia

3 Laboratory of Probabilities and Statistic, Faculty of Sciences of Sfax, University of Sfax, BP. 1171, 3000 Sfax, Tunisia

4 Departamento de Física de la Materia Condensada, Facultad de Ciencias, Universidad de Zaragoza, 50009 Zaragoza, Spain

5 Instituto de Nanociencia y Materiales de Aragón (INMA), CSIC-Universidad de Zaragoza, Campus Río Ebro, 50018 Zaragoza, Spain

Published online: 09 January 2025

along with decreased stability and sunlight penetration, can disrupt the biodiversity and balance of aquatic ecosystems. To address these issues, it is necessary to pre-treat effluents containing dyes before releasing them into the environment. In recent years, researchers have actively tested and developed various techniques for removing dyes from wastewater, including coagulation and chemical oxidation [3], biodegradation [4], ultrasonic degradation [5], photodegradation [6], membrane separation [7], and adsorption [8–10]. Among these methods, adsorption stands out as the most commonly used technique for removing dyes from aqueous solutions, thanks to its durability, cost-effectiveness, environmental friendliness, and simplicity. Adsorption-based materials are increasingly recognized as effective and sustainable solutions for combating water pollution, with innovative composites showing high efficiency in removing dyes and contaminants. Developing an adsorption system begins with selecting a suitable adsorbent from various available options. Additionally, dyes, which act as adsorbates, are typically classified based on their particle charge when dissolved in an aqueous medium [11, 12].

Advances in adsorption technology have emerged as a viable alternative for the removal of dyes and other pollutants from industrial wastewater. Various materials have been used to extract dyes from solutions, including carbon nanotubes, gypsum [13], zeolites [14], chitosan composites, solid waste, magnetic chitosan-sugar-graphene oxide composites [15], and magnetic lignin [16]. Organic dye molecules are highly resistant to oxidants and biological degradation, making chemical and biological water treatment methods impractical. Although numerous studies have explored adsorbents for the removal of either anionic or cationic dyes, research on methods capable of simultaneously removing both types remains limited.

Nanotechnology provides a vast array of possibilities for creating composite materials that combine organic and inorganic components with multifunctional properties to address this significant challenge. In particular, hybrid nanomaterials have emerged as highly efficient and promising adsorbents, offering a compelling alternative to conventional options. However, their efficacy in dye removal for wastewater treatment, although widespread, lags behind that of electrospun nanofiber membranes, thus limiting their applications [17–22]. Electrospun nanofiber membranes are particularly noteworthy among these nanomaterials due to their high surface area-to-weight ratio, flexibility, porosity, excellent water permeability, and easily modifiable surface properties [18, 23]. Consequently, wastewater treatment processes have started to focus more closely on their integration.

In recent years, nanofiber mats have garnered significant interest, primarily due to their outstanding advantages over traditional membranes, including a higher surface area-to-volume ratio and remarkable mechanical properties [23]. In the electrospinning process, high voltage is applied to counteract surface tension forces within a polymer solution, resulting in the rapid formation of fine fibers. As the solvent dries, it forms a network of small fibers typically measuring several hundred nanometers in diameter. The droplet adopts a conical shape at the tip of the syringe, where the polymer drop extends toward the grounded collector [24–28]. Notably, the presence of a substantial surface area in the nanofibers is a key factor contributing to their effectiveness as adsorbent surfaces [29, 30].

Mehdizadeh et al. demonstrated that embedding MNPs in polymeric matrices improved their dispersibility and reusability [31]. Reynel-Ávila et al. reported enhanced adsorption performance of MNPs when immobilized in carbon-based nanocomposites [32]. Electrospinning has recently gained attention as a facile method to fabricate nanofiber composites with MNPs. This technique allows for the production of nanofibers with controlled diameter and high surface area, providing an ideal platform for effective dye adsorption. Atikah et al. highlighted the advantages of electrospun nanofibers in wastewater treatment, noting their superior adsorption capacities compared to bulk materials [33].

Adsorption-based materials have emerged as effective and sustainable solutions for addressing water pollution, with various innovative composites demonstrating high performance in removing dyes and contaminants. For example, sugarcane bagasse-based biocomposites showed excellent efficiency in removing Acid Red 1 dye, with reversible adsorption properties and adherence to the Langmuir model, making them suitable for industrial wastewater treatment [34]. Similarly, nickel-doped MnO_2 nanorods supported on biochar from coconut shell and rice husk exhibited a high lithium adsorption capacity (89 mg g^{-1}) and a 98% desorption efficiency, offering promising potential for large-scale recovery applications [35]. Composite adsorbents combining biochar with metal oxides or nanoparticles have also demonstrated exceptional efficiency, selectivity, and reusability in dye and contaminant removal, following established adsorption models [36]. Additionally, advanced materials like yttrium and nickel-doped magnetite nanowires coated with mesoporous silica achieved rapid degradation of crystal violet dye under sunlight, reaching 90% degradation in just 10 min, with 99% magnetic separation efficiency, providing a robust solution for organic pollutant treatment [37]. Biomass-derived adsorbents have also shown great promise. Activated carbon prepared from *Sesbania sesban* stems exhibited a remarkable methylene blue adsorption capacity of 1380 mg g^{-1}, with spontaneous and exothermic adsorption, confirming its potential

for sustainable water treatment [38]. Similarly, Mg–Al layered double hydroxide (LDH) composites combined with *Mangifera indica* stone biomass achieved effective RG5 dye removal (73.5 mg g^{-1}) and demonstrated regeneration potential, highlighting their feasibility for eco-friendly wastewater management [39]. These studies emphasize the versatility and efficiency of advanced adsorbents, providing cost-effective and sustainable approaches for industrial and environmental wastewater treatment challenges.

Arshad et al. demonstrated that Mg^{2+}-doped zinc oxide nanofibers offer promising prospects for dye treatment due to their enhanced charge transport properties and stability. They also showed the efficient performance of electrospun TiO_2 and ZnO nanofibers in the photocatalytic degradation of dyes, providing interesting prospects for sustainable treatment of contaminated water [40, 41].

These properties make Electrospun Polymer Nanofibers (EPNFs) highly suitable for effectively adsorbing a range of pollutants, including heavy metals, dyes, and other contaminants. Currently, there is limited number of review articles available on EPNFs and their utilization in water treatment. The majority of these publications concentrate on the manufacturing and utilization of EPNFs in the realm of water treatment. They serve various purposes, acting as adsorbents and filters for diverse pollutants, acting as sensors for contaminant detection, or operating as nanocomposites for contaminant degradation [42, 43].

Recently, Pereao et al. conducted a study focusing on the application of EPNFs in water treatment, particularly in the removal of heavy metals [44]. Considering the unique properties of electrospun polymer nanofibers (EPNFs), an in-depth exploration of modification techniques and their influence on improving dye removal efficiency from aqueous solutions is essential. Such an investigation will enable researchers to identify innovative strategies for enhancing the performance of EPNFs as effective adsorbents for various toxic dyes while addressing the practical challenges associated with their real-world application.

The presence of Congo Red (CR) dye in water is considered unacceptable due to its inhibitory effect on the re-oxidation of water. Exposure to this contaminant can lead to eye and skin irritation, as well as symptoms like stomach pain, nausea, vomiting, and diarrhea [45–47]. The adsorption process has been used as a suitable model for the removal of CR. Consequently, a number of adsorbents with different adsorption capacities have been proposed. In addition, Toluidine Blue (TB) has emerged as a widely used substance in diverse fields including medicine, the textile industry, and biotechnology [19]. It finds applications as a mediator in various chemical or biochemical reactions such as a dye for fabrics, a photosensitizer for the study of light-activated microorganisms, and a marker for organism identification.

A key challenge in treating colored wastewater lies in the complexity of simultaneously removing dyes of different chemical natures, particularly anionic and cationic dyes, which interact differently with conventional adsorbents. Traditional methods are often limited by their selectivity, making it possible to remove only one type of dye at a time, necessitating additional steps or the use of multiple types of adsorbents. In this context, the use of magnetized nanofibers (MNFs) emerges as an innovative and promising solution. These MNFs possess unique properties, such as high specific surface area, chemical compatibility, and ease of recovery due to their magnetic responsiveness. These characteristics enable not only efficient adsorption but also the possibility of simultaneous removal of both anionic and cationic dyes under optimized conditions. By integrating magnetic nanoparticles into a nanofiber matrix, this approach offers a multifunctional system capable of addressing the complexity of industrial effluents.

This study will present an innovative approach for treating dye-contaminated water using a composite material made of magnetite nanoparticles immobilized in nanofibers. The nanofibers are expected to demonstrate enhanced adsorption capacity, with favorable physicochemical characteristics. This innovative approach will be evaluated for its effectiveness in removing various dyes, highlighting the considerable potential of magnetite nanofibers as efficient adsorbents. This method promises to offer an eco-friendly and cost-effective solution for treating industrial wastewater, particularly from dye-laden textile industries.

The novelty of this work lies in the development of a composite material combining magnetite nanoparticles (MNPs) with electrospun polymer nanofibers (EPNFs) to create a multifunctional adsorbent capable of simultaneously removing both anionic and cationic dyes. While previous studies have extensively explored single-component adsorbents for either cationic or anionic dyes, this study addresses the gap in simultaneous removal, optimizing the adsorption process for complex dye mixtures. Furthermore, the integration of MNPs within nanofibers enhances both the adsorption capacity and reusability of the material, offering a sustainable, eco-friendly, and cost-effective solution for industrial wastewater treatment. By systematically evaluating the effects of key parameters such as contact time, adsorbent dosage, and dye concentration, this work provides a comprehensive framework for the practical application of magnetic composite nanofibers in water pollution management, thereby advancing the field of wastewater treatment.

The aim of this study is to prepare magnetic composite nanofibers using the electrospinning method and magnetic nanoparticles and their identification. Subsequently, an

evaluation was carried out to assess the potential adsorption capacity of these composite nanofibers for the treatment of organic pollutants.

The primary objective was to demonstrate the efficiency of magnetic nanofibers in the treatment of water pollution, with a particular focus on the cationic dye TB and the anionic dye CR. The effect of various factors on the adsorption process such as contact time, the amount of used adsorbent and the concentration of the dyes was evaluated. The aim was to provide a detailed understanding of the adsorption process and to optimize the conditions for maximum dye removal efficiency.

2 Materials and Methods

2.1 Chemicals and Reagents

Polyacrylonitrile (PAN, C_3H_3N, Mw = 150,000) powder and N, N-dimethylformamide (DMF, $CHON(CH_3)_2$) high-purity reagent plus 99% sourced from Sigma-Aldrich (USA). Colorants hydrated TB conforms to the analytical standards of CI 52,040 MIC and hydrated CR meets the analytical standards of CI 22,120 from Labbox Labware, S.L (Spain). Milli-Q deionized water with a resistivity of 18.2 MΩ cm was used in the experiments.

2.2 Materials Synthesis

The employed MNPs belong to the same batch of samples obtained using the combustion synthesis process described in our previous work [45]. For the elaboration, characterization and evaluation of the hybrid membrane composed by a polymeric matrix containing MNPs (referred to as MNF samples), the procedures are described as follows.

2.3 Embedding of Nanoparticles within Nanofibers by Electrospining

The materials processing for the elaboration of the MNFs is schematized in Fig. 1. This methodology is based in a laboratory-made electrospinning system, whereof details can be consulted in [35]. For the precursor solution preparation, 1 g of MNPs was added to 10 mL of DMF and the mixture, sonicated for 10 min in an ultrasonic bath for homogeneous dispersion. Then, was placed on a heating plate with magnetic stirring (80 °C, 250 rpm) to enhance the solubility of the polymer. Afterwards, 1 g of PAN was dissolved in the DMF-MNP mixture under stirring and heating over a span of 2 h. The heat was then turned off and the stirring continued for an additional 12 h (Fig. 1a).

To ensure reproducibility, the electrospinning process was repeated in triplicate under the same operating conditions, and the obtained MNFs were compared to confirm consistency in morphology and yield. To produce hybrid polymer membranes composed of PAN and MNP (MNF), the precursor solution was charged into a plastic syringe (10 mL) to be placed in the electrospinning apparatus (Fig. 1b). The feeding rate of 0.7 mL/h was maintained until reaching 1 mL of solution. The working distance was 15 cm and the applied voltage 8 kV. The obtained MNFs were dried (180 °C, 12 h) in air atmosphere.

2.4 Characterization Techniques

The obtained MNFs underwent characterization using various analytical techniques. Scanning Electron Microscopy (SEM) was performed using an Inspect F50 (Thermo Fisher Scientific, USA) for morphological analysis, and ImageJ software for processing and analyzing scientific images was utilized for image processing and average size determination. The samples were coated with a 20 nm carbon layer

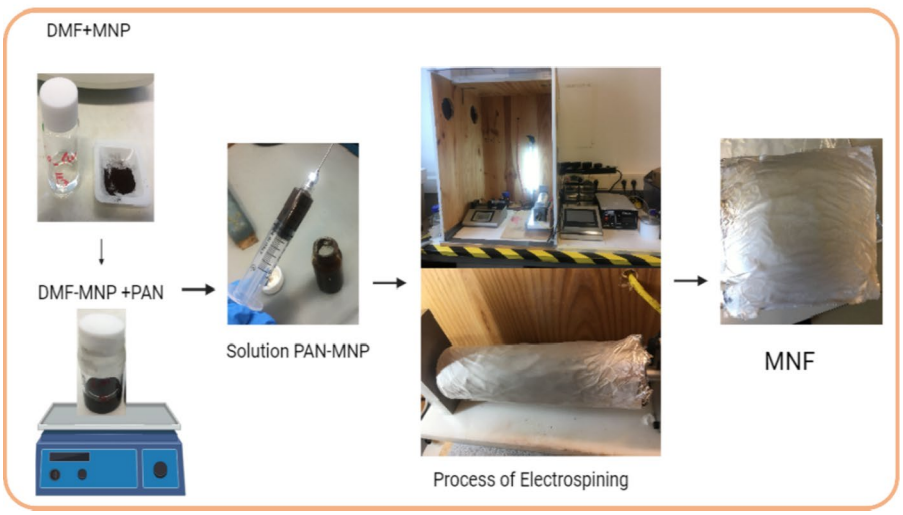

Fig. 1 Organic matrix (polyacrylonitrile, PAN) with inorganic particles (magnetite, MNP) hybrid membrane´s (MNFs) elaboration using electrospinning processing. MNP were dispersed in a suitable solvent (dimethylformamide, DMF), the dispersion was heated and mixed with PAN powder. After overnight stirring at room temperature, the solution was electrospunned and the obtained fibers collected in an aluminum foil

using an evaporative carbon coater (Leica EM ACE600, Leica Microsystems, Germany). Fourier Transform Infrared Spectroscopy (FTIR) was carried out with a Vertex 70 spectrometer (Bruker, Germany) to investigate the chemical composition of the samples. Thermal analysis of the MNFs was conducted using thermogravimetric analysis (TGA) with a TGA/SDTA851 analyzer, operating from 50 to 800 °C at a heating rate of 10 °C/min. Surface area and porosity were determined using a TriStar II 3020 system (Micromeritics, USA) in combination with a VacPrep 061 sample degassing system (Micromeritics, USA).

2.5 Evaluation of the MNFs as Adsorbates for Ionic Dyes

For the sorption experiments, initial dye solutions were prepared at a concentration of 500 mg L^{-1}. The study aimed to evaluate the adsorption efficiency of MNP and MNF for CR (anionic dye) and TB (cationic dye) at initial concentrations of 2 mg L^{-1} and 10 mg L^{-1}, respectively. The experiments were conducted in a controlled environment at a constant temperature of 20 °C over a duration of 10 h. During these experiments, the amount of adsorbent varied from 0.5 g L^{-1} to 3 g L^{-1}. This variation allowed for the determination of the optimal amount and contact time for adsorption by monitoring changes in the dyes' absorbance. Absorbance was measured using a Shimadzu UV-1280 UV–Vis spectrophotometer at the dyes' maximum absorption wavelength, applying the following equation:

$$\text{Removal efficiency} = \frac{(C_0 - C_e)}{C_0} \times 100 \quad (1)$$

where C_0 is the initial concentration of the substance to be adsorbed (mg L^{-1}). C_e is the final concentration of the substance to be adsorbed (mg L^{-1}).

2.5.1 Calibration Curve for Colorants

The concentrations of TB and CR solutions were varied between 0.02 and 2 mg L^{-1} and 2–10 mg L^{-1}, respectively. The absorbance of TB (632 nm) and CR (498 nm) at different concentrations was measured using a UV spectrophotometer, with calibration curves for TB and CR in Figs. 2 and 3, respectively.

The resulting UV-Vis absorbance spectrum was plotted and analyzed to determine the absorbance-concentration relationship indicating that Beer's Law holds for this system [42]. A linear regression analysis was performed using the data to obtain the equation y = a + bx, where y represents the absorbance and x represents the concentration of TB and CR. The intercept of the equation was found to be 0.03185 ± 9.66175E−4 for TB and 0.00291 ± 0.00661 for CR and the slope was found to be 0.00792 ± 1.02491E−4 to TB and 0.03153 ± 0.0014 for CR. The R^2 value, which indicates the goodness of fit of the regression line, was found to be 0.99933 for TB and 0.99607 for the CR, indicating a very strong correlation between absorbance and concentration. The derived equation can be used to calculate the concentration of an unknown sample of Toluidine Blue or Congo Red by measuring its absorbance and substituting the value into the equation. This allows for precise determination of the sample's concentration.

$$\text{Concentration} = \frac{\text{ABS} - \text{Intrcept}}{\text{Slope}} \quad (2)$$

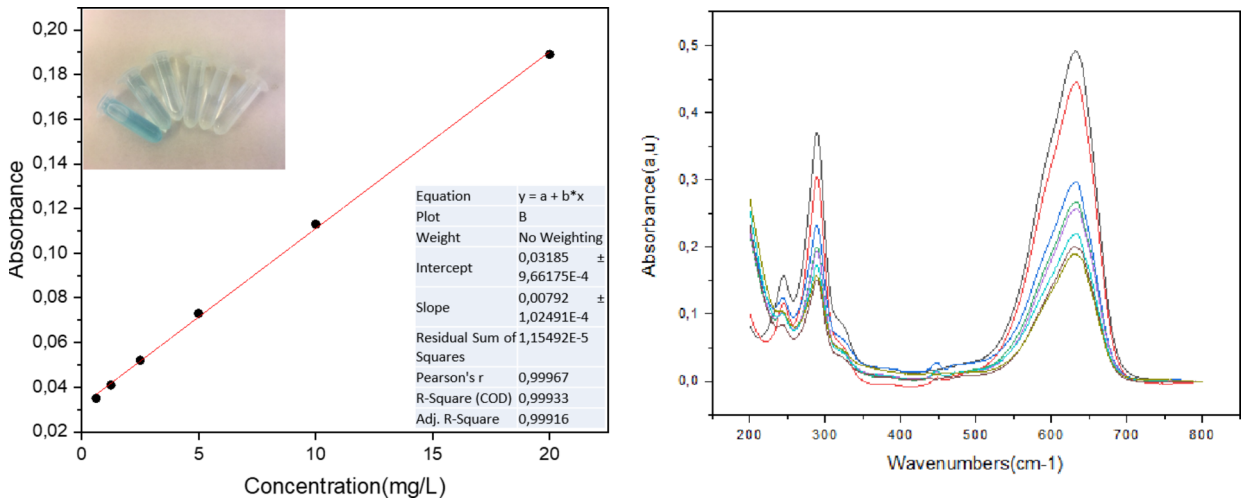

Fig. 2 Calibration curve and UV-Vis absorption spectra for toluidine blue concentration determination

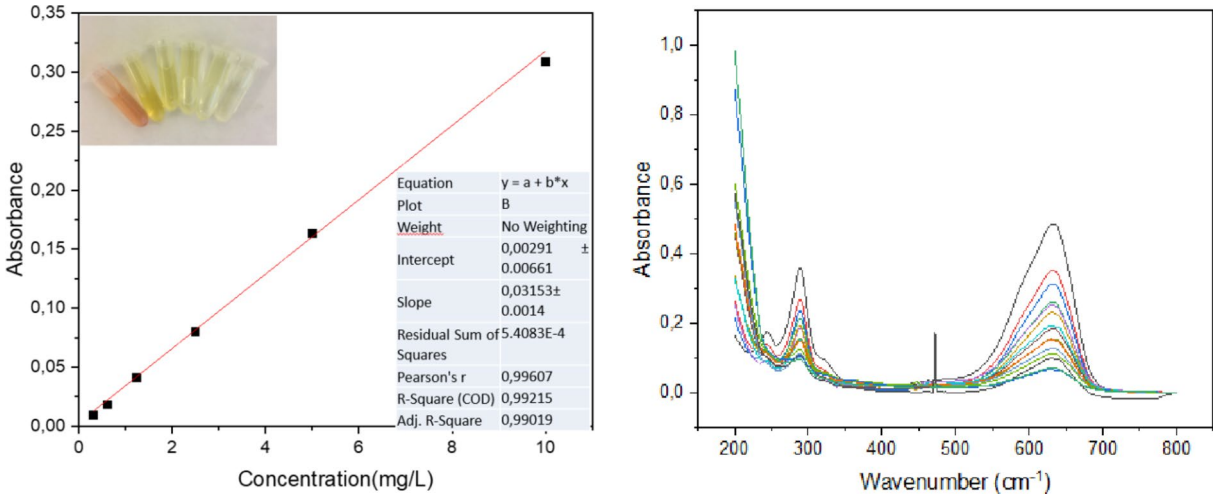

Fig. 3 Calibration curve and UV-Vis absorption spectra for Congo red concentration determination

According to Coelho et al. (2008), the R^2 value of 0.9961 obtained for the calibration curve of Toluidine Blue (TB) indicates a strong and reliable relationship between the amount of TB and the measured absorbance [48].

2.5.2 Theoretical Analysis and Modelling

Various adsorption kinetic models have been employed to assess the performance of the adsorbent and to examine the mechanisms of adsorption mass transfer [49]. Understanding adsorption kinetics is crucial for designing an effective adsorption system. These models help predict the pollutant removal rate, determine the time-dependent concentration of the remaining adsorbate in the solution, and elucidate the underlying mechanisms of the adsorption process, which are essential for evaluating the efficiency of the adsorbent used [50].

Various adsorption kinetic models have been developed and applied to describe the adsorption kinetics such as pseudo-first-order (PFO) model [51], the pseudo-second-order (PSO) model [52, 53], the mixed-order (MO) model [50], the Langmuir kinetic model [54, 55], the Elovich model [49] and the phenomenological mass transfer models [56–58]. Among them, the PFO and PSO models are the most frequently used to description the adsorption kinetic process [50]. They are derived by Liu and Shen from the Langmuir kinetics and they suggested that the PFO and PSO kinetic was related to the values of equilibrium fraction of adsorbent active sites and the ratio of the pseudo-first- and–second-order rate constants [59]. It is reported by [60] that the PFO and PSO models were capable of modeling the adsorption kinetic at high and low initial adsorbate concentration, respectively. Ho suggested that the PSO model is suitable for representing the chemisorption process [61]. According to a recent study made by Khamizov, it is concluded that the applicability of the PSO model is independent of the mechanisms determining the rate of sorption and does not require concepts of chemisorption or special equations of kinetics controlled via chemical reactions or diffusion. It is stated that the kinetic model of sorption based on a PSO equation become extraordinarily popular after works of Ho and McKay [62].

2.5.3 Pseudo-Second-Order Kinetics Model

The pseudo-second order model suggests the existence of chemisorption [52] based an electron exchange for example between the adsorbate molecule and the solid adsorbent [63]. The pseudo-second-order kinetic model assumes that the rate-controlling step is likely chemisorption, which involves valence forces through the sharing or exchange of electrons between the adsorbent and the adsorbate [63]. It is represented by the following expression:

$$\frac{dq}{dt} = k_2 \cdot (q_e - q_t)^2 \tag{3}$$

Integrating the equation gives:

$$\frac{t}{q_t} = \frac{1}{K_2 \cdot q_e^2} + \frac{1}{q_e} \cdot t \tag{4}$$

k_2: the rate constant for second-order kinetics (mg g^{-1} min^{-1}). q_t: the adsorption capacity at time t (mg g^{-1}). q_e: adsorption capacity at equilibrium (mg g^{-1}).

The Nash–Sutcliffe model efficiency coefficient (NSE) was employed to compare the predictive skill of hydrological models. coefficient criterion as hypothesis testing indicator, using root mean square error (RMSE) and standard deviation (SD) as follows $\mathrm{NS} = 1 - \left(\frac{\mathrm{RSME}}{\mathrm{SD}}\right)^2$. This

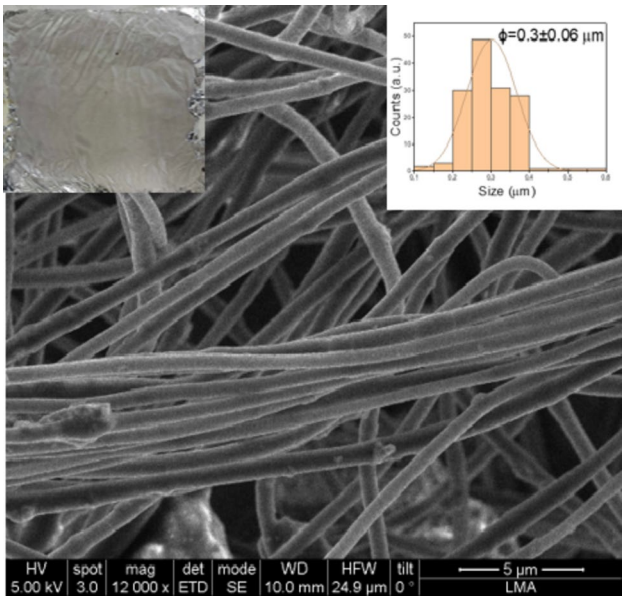

Fig. 4 SEM image of the composite MNFs. The surface of the membranes shown that it is composed by fibers with average diameter of 0.3 ± 0.06 µm

coefficient of efficiency of mathematical predictions has a perfect fit at NSE = 1 [64].

3 Results

3.1 Morphological Characterization

Typical SEM micrography from the obtained MNFs shown that the matrix is composed by fibers with average diameter ϕ = 0.3 ± 0.06 µm (Fig. 4), as well as the presence of some MNPs agglomerates in the surface of the samples. Adequate parameters in the conditions during the electrospinning process were employed for the homogeneous average diameter in the elaborated MNFs.

Despite the high concentration of MNPs in the precursor solution, the samples exhibited a homogeneous dispersion of inorganic particles within the organic matrix, demonstrating that the hybrid material was successfully fabricated and that the morphological properties of the composites were well-controlled. The surface roughness, as observed in SEM images, is primarily attributed to the presence of MNP agglomerates on the fiber surfaces. This roughness likely increases the available surface area, facilitating enhanced interactions with adsorbate molecules. The uniform fiber diameter and the rough surface texture work together to optimize adsorption performance by providing a high surface area-to-volume ratio and a homogeneous distribution of active adsorption sites.

3.2 BET Surface Area Analysis

The specific surface area of the elaborated magnetic composites is a crucial parameter on the ability to adsorb pollutants from water and remove various molecules. Based on the isotherms depicted in Fig. 5, the MNFs exhibit a behavior of Type III (IUPAC) isotherms. Characterized by rapid exponential increase in the adsorption uptake at the start of increase in the pressure/concentration, the isotherm in Fig. 5 shows the equilibrium uptake of adsorbate-adsorbent (N_2-MNFs) pair, related to a physical adsorption phenomenon. In this case, can be consider that the N_2 molecules were accommodated on the surface of the MNFs in mono- or multilayer formations, providing them favorable energy state.

The measured BET surface area for MNFs was found to be 9.9457 ± 0.0363 $m^2\ g^{-1}$, with a pore volume of approximately 0.02 $cm^3\ g^{-1}$ and a pore size of 8.778 nm. These pore

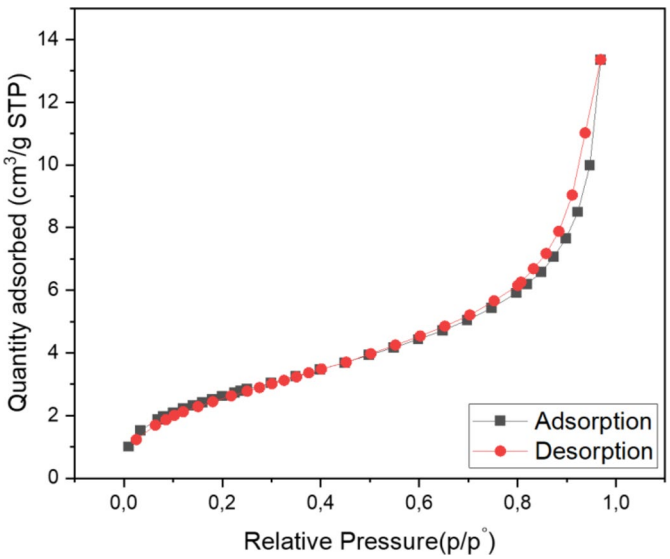

Fig. 5 BET isotherm form the MNFs composites. The N_2 adsorption-desorption isotherm exhibit type II behavior

size distribution and surface heterogeneity cause a unique interaction of each adsorbate-adsorbent pair.

The specific surface area of 9.9457 ± 0.0363 m^2 g^{-1} and the pore size of 8.778 nm suggest that the MNFs provide a surface suitable for adsorption processes. The Type III isotherm indicates that adsorption primarily occurs through weak physical interactions, such as van der Waals forces, between the adsorbent and adsorbate. These physical interactions are characteristic of non-porous or macroporous materials, where the adsorption sites are predominantly located on the external surface. The heterogeneous pore distribution enhances the ability of the MNFs to interact with a variety of adsorbate molecules, making them versatile for pollutant removal. The pore size and volume further suggest that the MNFs are suitable for adsorbing molecules of intermediate size, ensuring efficient adsorption performance in aqueous systems.

The heterogeneous pore distribution further enhances the versatility of the MNFs, enabling them to interact effectively with a wide variety of adsorbate molecules, including both cationic and anionic dyes. The mesoporous structure (2–50 nm) ensures compatibility with molecules of intermediate size, such as Toluidine Blue (~1.3 nm) and Congo Red (~2 nm), allowing efficient diffusion and adsorption in aqueous systems. Additionally, the combination of moderate surface area, pore size, and heterogeneous pore distribution facilitates rapid adsorption kinetics and high removal efficiencies, making MNFs highly practical for real-world applications in wastewater treatment.

Additionally, the moderate surface area and pore size distribution make the MNFs particularly effective for the adsorption of organic pollutants and larger molecular compounds. The external surface and accessible pores provide active sites where adsorption can occur, driven by the compatibility between the pore size and the dimensions of the adsorbate molecules. The heterogeneous pore distribution further enhances the ability of the MNFs to interact with a wide range of contaminants, ensuring efficient adsorption. This versatility makes the MNFs suitable for removing pollutants with varying molecular sizes and chemical properties in aqueous environments.

3.3 Thermal Analysis

The MNFs shown the thermal behavior presented in Fig. 6.

The examination of the thermogram highlights three distinct phases of mass loss in the sample. During the first phase, ranging from 50 to 250 °C, a gradual and slow mass loss occurs, reaching 1%. This stage is often associated with the desorption of water and the release of adsorbed gases, which reflects the ability of the MNFs to retain their stability under mild thermal conditions. The second phase is characterized by a more substantial mass loss. Between 250 and 350 °C, a 20% reduction is observed, suggesting the decomposition of some organic components and/or structural transformations. Such changes may influence the availability or stability of active sites critical for adsorption processes. The third phase is marked by a rapid mass loss, extending from 350 to 600 °C with a reduction reaching 99%. This stage indicates a complete decomposition of residual components, possibly affecting the long-term thermal resilience of the material. Beyond these temperatures, the mass of the magnetite nanofibers almost completely stabilizes, marking the end of major thermal transformations.

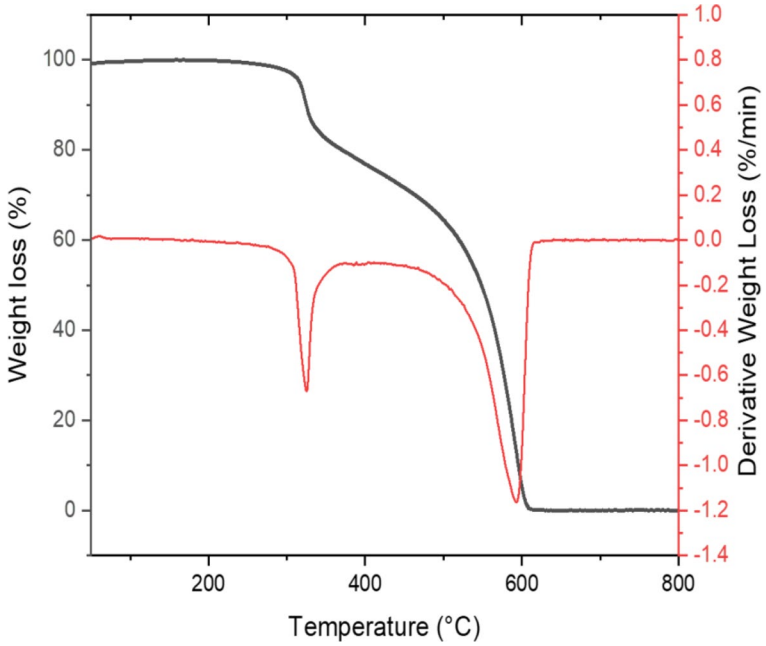

Fig. 6 Thermogram of the elaborated MNFs

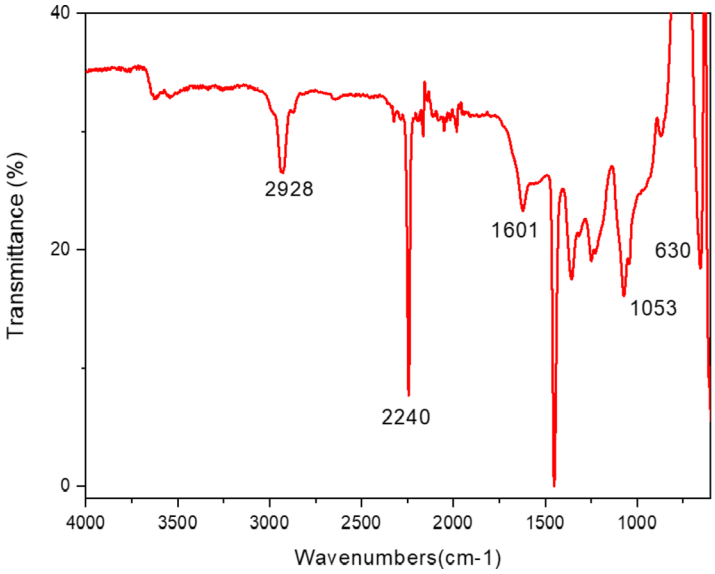

Fig. 7 FTIR spectrum from the MNFs, showing the interactions from the composites

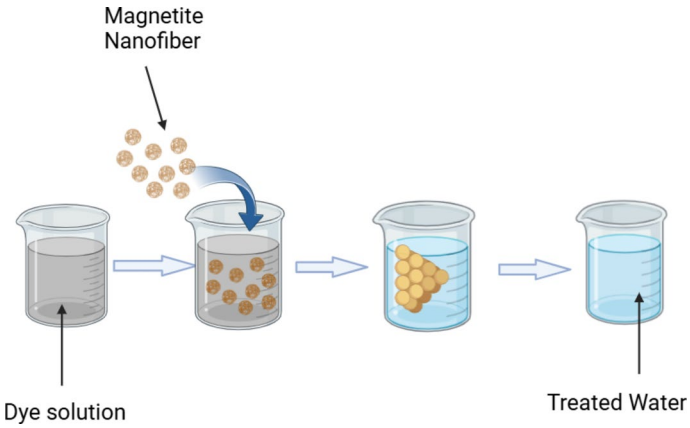

Fig. 8 Adsorption mechanism of dyes on MNFs adsorbent

This stabilization is crucial for maintaining the structural integrity of the MNFs during high-temperature regeneration processes often required in adsorption applications. Additionally, an exothermic peak observed around 600 °C signals a phase transition from Fe_3O_4 to Fe_2O_3, which may alter the magnetic properties and impact the material's performance in adsorption-based separations.

3.4 FTIR Spectra

During the examination of the FTIR spectrum, prominent absorption bands was observed in Fig. 7 at 630 cm^{-1}. These bands are indicative of the stretching vibrations of Fe–O functional groups, confirming the crystalline lattice structure of magnetite (Fe_3O_4), as documented in previous studies [60]. The work of Venkateswarlu et al [65], validates the concept that magnetite can create interconnected crystal structures, with atoms connected via balanced forces such as ionic, covalent, or van der Waals bonds. The observed data suggests that the vibrational behaviors of the Fe–O bond correlate with octahedral and tetrahedral sites, manifesting at approximately 540 cm^{-1} and 660 cm^{-1}.

An intense band at approximately 2928 cm^{-1} indicate the presence of C–H stretching associated with aliphatic hydrocarbons. Subsequent bands at 1601 cm^{-1}can be ascribed to C=O or C=C bond vibrations. The observed peaks at 2240 cm^{-1}suggest the presence triple bonds, such as C≡N. Additionally, bands proximate to 1053 cm^{-1} represent C–O bond vibrations.

The presence of these functional groups plays a critical role in the adsorption process. Fe–O groups in the magnetite structure provide active sites for electrostatic interactions with ionic or polar contaminants, particularly inorganic pollutants. Similarly, C=O and C≡N groups can form hydrogen bonds or dipole–dipole interactions with organic molecules, enhancing the adsorption of aromatic and polar compounds. The C–O bonds contribute to chemical binding with specific adsorbates, further increasing the versatility of MNFs for pollutant removal. Collectively, these functional groups impart chemical reactivity to the surface of MNFs, enabling

the adsorption of a diverse range of organic and inorganic pollutants in aqueous systems.

4 Evaluation of the MNFs as Adsorbents for Ionic Colorants

4.1 Adsorption's Performance of MNFs

4.1.1 Comparative Study of the MNPs and MNFs Performance Removing Dyes

The adsorption mechanism of dyes onto MNFs, as illustrated in Fig. 8, involves both physical and chemical interactions. Physical adsorption is primarily driven by Van der Waals forces between the dye molecules and the surfaces of the nanofibers, facilitated by the high specific surface area and porous structure of the MNFs. Chemical adsorption may also play a significant role, with the formation of chemical bonds between the functional groups present on the MNFs and the dye molecules. Furthermore, the presence of magnetite nanoparticles embedded in the nanofibers can enhance adsorption through magnetic interactions, contributing to a more efficient dye capture process.

The evaluation begins by analyzing the enhanced performance of the electrospun composite nanofibers (MNFs) compared to the native inorganic nanoparticles (MNPs). A comparative study of the adsorption rate was conducted using 1 g L^{-1} of adsorbent, based on UV–Vis spectroscopic analysis of the ionic dye concentration in the solution over time. By monitoring the characteristic absorption peaks of TB and CR solutions containing the adsorbent, experimental adsorption rate curves were generated to compare the performance of the MNPs and the MNFs as adsorbents over a 10 h incubation period.

The comparative adsorption rate curves using both adsorbents (MNPs and MNFs) are presented in Fig. 9a for TB and Fig. 9b for CR, respectively. For TB dye, the use of MNFs achieved removal efficiency rate of 86%, while MNP achieved a removal efficiency rate of 65%. Meanwhile, in the case of CR, the 79% of CR was removed (Fig. 8b), while MNPs only achieved a 64%. Composite MNFs underscores superior performance in the removal of ionic dyes from aqueous solutions based on this significant difference. According to Wang et al., the g-C_3N_4/Nb_2O_5 nanofibers prepared through electrospinning are highly effective for removing organic pollutants from water. These nanofibers showed a remarkable ability to break down pollutants such as rhodamine B and phenol when exposed to visible light. Additionally, their unique structure makes them easy to retrieve and reuse in the water treatment process [67]. The study conducted by Li et al. highlights the development of an innovative membrane based on PAN-ZnO nanofibers, revealing exceptional potential for water treatment and organic pollutant degradation. This membrane exhibits a dye removal rate of over 90% after 10 h of continuous electrocatalytic filtration [68]. This suggests that the use of composite electrospun nanofibers could be a practical and efficient solution for cleaning up organic pollutants from water [69].

4.2 MNFs Adsorption Capacity for Cationic Dye

The study focused on assessing the effectiveness of the composite MNFs as adsorbents for the TB´s removal in function of the determined mass (0.5/0.75/1/2 and 3 g L^{-1}) (Fig. 10). The results demonstrated a positive correlation between the mass of nanofibers and the removal efficiency of TB. At the lowest concentration of 0.5 g L^{-1} (MNFs1), the 54% of the TB´s concentration was reduced, emphasizing the

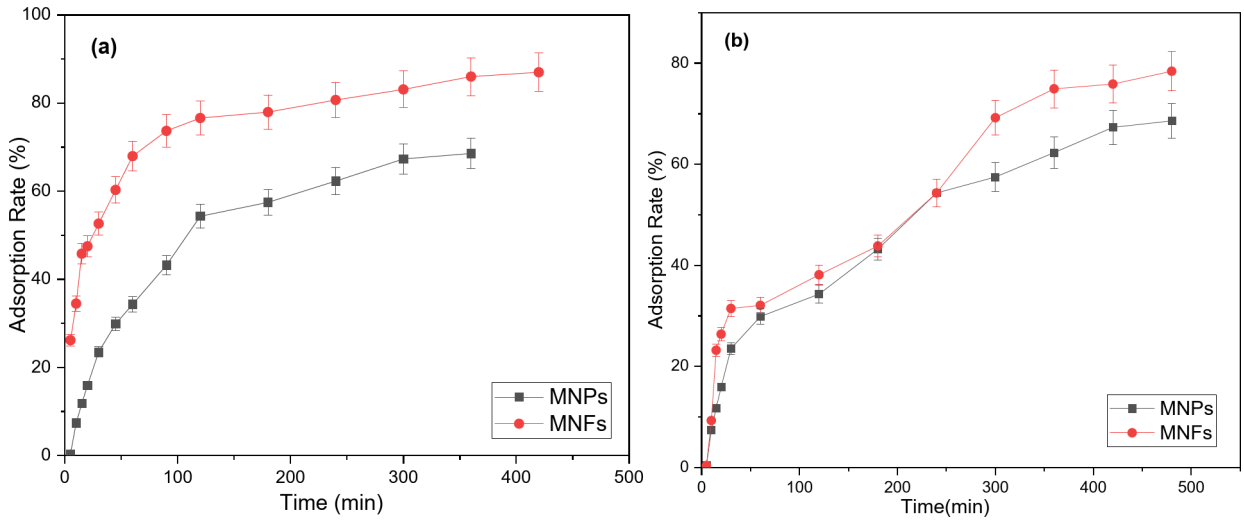

Fig. 9 Comparative adsorption rate curves using MNPs and MNFs (1 g L^{-1}) for cationic toluidine blue (a) and anionic Congo Red (b) organic dyes

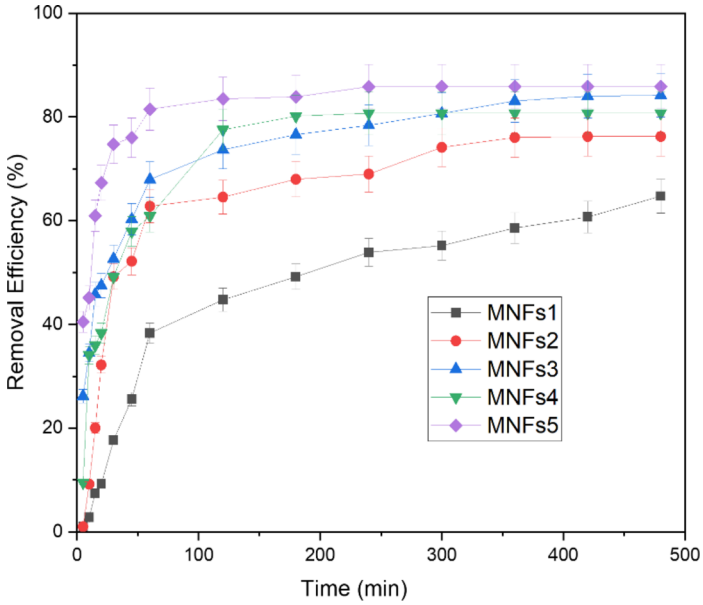

Fig. 10 Impact of MNF mass on the removal efficiency of toluidine blue

significant efficiency of MNFs even using reduced mass of adsorbent. As the mass of MNFs is increased, enhanced efficiency was observed. MNFs as adsorbents for TB are capable reduce its concentration in a 69% using 0.75 g L^{-1} (MNFs2) and reach 78.4% for 1 g L^{-1} (MNFs3).

Further increases in mass to 2 g L^{-1} (MNFs4) and 3 g L^{-1} (MNFs5) resulted in only slight improvements, with elimination rates of 80.17% and 82.85%, respectively. However, a tendency was observed where the time required to achieve maximum removal efficiency decreased. Therefore, the modest increase in efficiency between MNFs4 and MNFs5 suggests that beyond a certain threshold, active sites are occupied by TB molecules, indicating the saturation of adsorption sites, and reducing its adsorption capacities. Based on these observations, the optimal mass of MNFs for effective removal appears to be approximately 1 g L^{-1}, corresponding to a removal efficiency of 78.4%. Beyond this mass, the improvement in elimination efficiency becomes marginal, suggesting a potential saturation point in the MNFs' removal capacity.

In a study conducted by Huong et al., polyacrylonitrile (PAN) nanofiber membranes were functionalized with bovine serum albumin (BSA), resulting in the formation of P-COOH-BSA nanofibers. These nanofibers were evaluated for their efficacy in removing Toluidine Blue O (TBO), a cationic dye, from wastewater. The findings revealed that P-COOH-BSA nanofibers exhibited significant removal efficiency, maintaining approximately 69% removal efficiency even after five adsorption/desorption cycles [69].

Nady et al. explore the use of electrospun nanofibers made from blends of polybutylene succinate and sulfonated expanded polystyrene for the removal of methylene blue [70]. Peydayesh et al. [71] describes the development of environmentally friendly, polymeric nanofibers made from polyvinyl alcohol and poly sodium acrylate. These nanofibers were used to remove cationic dyes like methylene blue from water. These nanofibers demonstrated efficient dye removal and maintained their adsorption capacity even after multiple reuse cycles [71].

4.3 MNFs Adsorption Capacity for Anionic Dye

In the case of CR organic colorant, the observed responses during the evaluation of the MNFs as adsorbents are quite similar to the cationic (TB) dye. As can be observed in Fig. 10, at the lowest concentration of 0.5 g L^{-1} (MNFs(a)), an elimination rate of 55% was recorded, underscoring the significant efficiency of MNFs as adsorbents for both colorants. Moreover, as the mass, a heightened efficiency was observed, achieving concentration reductions up to 67% for MNFs(b) at 0.75 g L^{-1} and reaching 79% of discoloration for MNFs(c) at 1 g L^{-1}.

Further increments in mass to 2 g L^{-1} (MNFs(d)) and 3 g L^{-1} (MNFs(e)) resulted in only marginal improvements, with elimination rates of 79% and 81%, respectively. The anionic dye´s saturation on the surface of MNFs represents the principal phenomena that limits the capacity to remove ionic molecules from water. Furthermore, MNF composite materials demonstrated enhanced removal efficiency compared to MNPs alone, showcasing their potential for pollutant remediation. These materials have exhibited promising responses in removing various contaminants. Das et al. [72] investigated the use of magnetic Fe^0/polyaniline nanofibers for the removal of CR dye through sonocatalysis, testing multiple conditions and achieving significant dye degradation. Similarly, Abid et al. [73] developed halloysite-TiO_2

nanocomposite fibers for the photocatalytic degradation of acetaminophen, emphasizing the critical role of the nanocomposites' chemical and physical properties in optimizing process efficiency. Phan et al. [74] explored the application of composite nanofibers in treating Reactive Black 5 (RB5) and Ponceau 4R (P4R), demonstrating their effectiveness in eliminating organic pollutants from industrial wastewater. Jiang et al. have demonstrated that the PLLA/CS-GO/TiO_2 composite nanofibers have a high saturated removal capacity of 74% for the organic dye CR, thus demonstrating the effectiveness of this treatment method for this specific pollutant [75].

The enhanced adsorption or degradation properties of these composite materials compared to individual nanofibers or nanoparticles can be attributed to their synergistic effects. The combination of different materials in the composites provides a larger surface area and more active sites for adsorption or catalytic reactions. Additionally, composite materials often show enhanced stability and reusability, thanks to the support provided by the nanofibrous matrix, which helps prevent the aggregation or leaching of active components. Moreover, the incorporation of magnetic components in the composites allows for easy separation from the treated water using a magnetic field, further improving the practicality and efficiency of the removal process (Fig. 11).

4.4 Adsorption Kinetics Studies

After identifying the optimal conditions for water treatment, the following parameters were defined: a contact time of 4 h, a concentration of 1 g L^{-1} of magnetite nanofibers (MNF), a pH of 8, a mixing speed of 200 rpm, and a temperature of 20 °C. These parameters were selected to maximize the adsorption efficiency of ionic dyes by MNF. A contact time of 4 h ensures equilibrium adsorption, while a concentration of 1 g L^{-1} of MNF provides a sufficient amount of available adsorption sites. A pH of 8 was chosen because it optimizes the interaction between the dyes and the MNF, promoting maximum adsorption. A mixing speed of 200 rpm ensures a homogeneous distribution of MNF in the solution, and a temperature of 20 °C is close to ambient conditions, facilitating practical application. To confirm the effectiveness of these parameters, adsorption kinetics studies were conducted under these specific conditions.

The TB´s adsorption isotherms obtained using MNFs as sorbents demonstrates a significant and direct correlation between the employed amount of MNFs and the dye adsorption effectiveness (Fig. 12). As the MNFs increased from 0.5 to 3 g L^{-1}, there is a notable modification in its adsorption behavior. The isotherms suggests that higher concentrations of MNFs in the solution provide more active sites for adsorption, thereby enabling more efficient dye molecule capture, reaching the equilibrium at reduced times.

Correspondingly, the k_2 rate constants for the PSO fitting (Table 1) shown a similar upward trend, rising from 0.38 to 24.13 mg g^{-1} min^{-1}. This progression suggests that the adsorption process accelerates, shortening the time required to reach equilibrium and emphasizing the potential of these materials as efficient adsorbents for dye removal. However, as the concentration of MNFs increases, the amount of adsorbed TB at equilibrium (qe in Table 1) significantly decreases, from 2.97 to 0.59 mg g^{-1}. The goodness of fit to the experimental data, evaluated using the NSE coefficient, demonstrates good predictive accuracy (NSE ≈ 1).

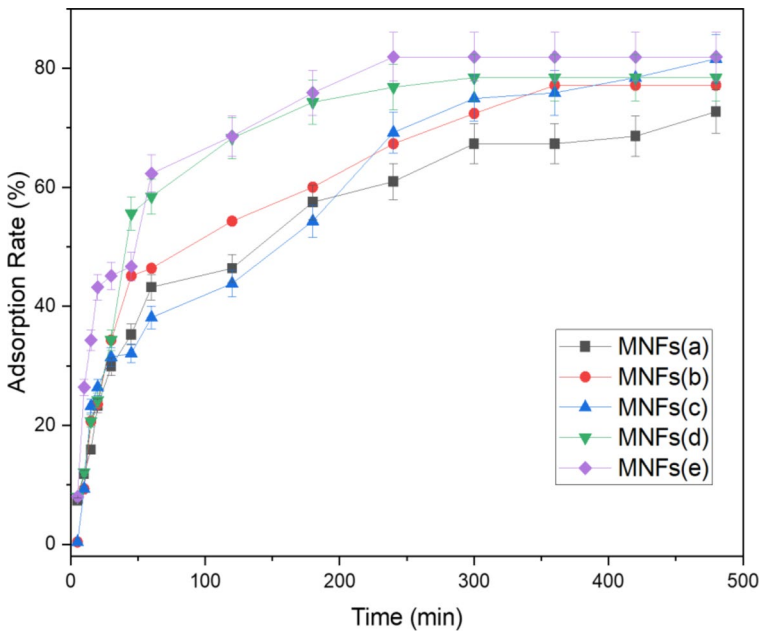

Fig. 11 Impact of the MNFs mass on the removal efficiency of Congo Red

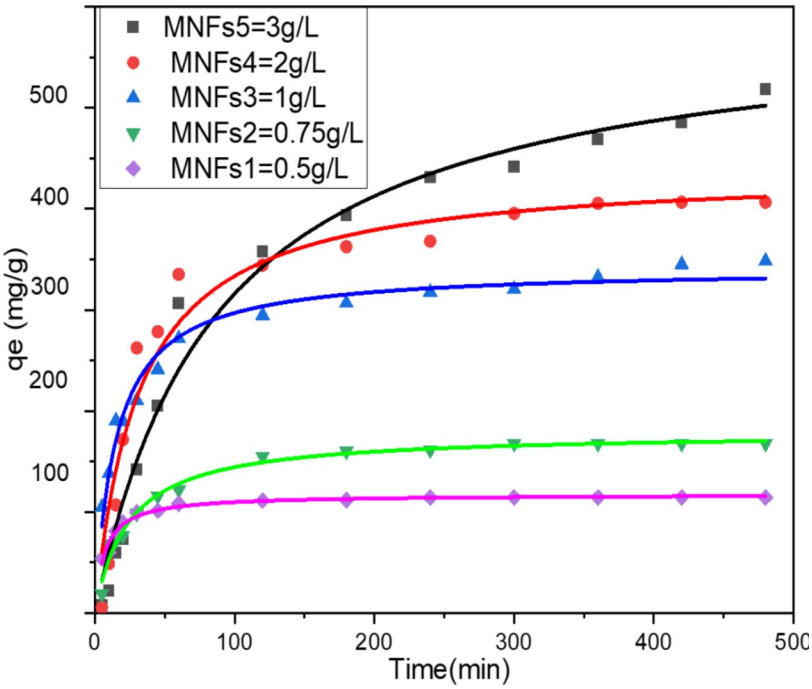

Fig. 12 Adsorption dynamics of TB using MNFs at different adsorbent concentrations

Table 1 Pseudo-second-order (PSO) kinetic fitting parameters for the TB´s experimental adsorption isotherms using different amounts of MNFs (0.5–3 g L^{-1})

Samples	$k_2 \times 10^{-2}$ (mg g^{-1} min^{-1})	q_e (mg g^{-1})	NSE	RMSE	SD_{exp}	SD_{PSO}
MNFs5	0.38	2.97	0.9784	0.0650	0.4699	0.4430
MNFs4	1.40	2.20	0.9407	0.1139	0.5248	0.4682
MNFs3	3.90	1.70	0.9780	0.0604	0.3976	0.4078
MNFs2	4.50	0.90	0.9844	0.0593	0.4842	0.4762
MNFs1	24.13	0.59	0.9785	0.0473	0.3258	0.3230

Table 2 Pseudo-second-order (PSO) kinetic fitting parameters for the CR´s experimental adsorption isotherms using different amounts of MNFs (0.5–3 g L^{-1})

Samples	$k_2 \times 10^{-2}$ (mg g^{-1} min^{-1})	q_e (mg g^{-1})	NSE	RMSE	SDexp	SD_{PSO}
MNFs(e)	0.12	15.41	0.9880	0.2522	2.2985	2.3112
MNFs(d)	0.18	11.04	0.9770	0.3749	2.6313	2.4731
MNFs(c)	0.14	9.07	0.9578	0.0604	2.6973	2.7195
MNFs(b)	0.48	4.63	0.9811	0.3536	2.7149	2.5740
MNFs(a)	1.26	2.92	0.9775	0.3530	2.4073	3.559

Cheng et al. investigated the adsorption of Methylene Blue by polydopamine-modified cellulose acetate nanofibers. Their results demonstrated a significant adsorption capacity, reaching up to 88.2 mg g^{-1} at a temperature of 25 °C and a pH of 6.5 after 30 h of adsorption. Additionally, the researchers conducted an analysis of pseudo-second-order kinetic constants, revealing a specific kinetic constant of 0.026 g/mg min for this process [76]. Mohammad et al. [78] investigated the adsorption of methylene blue onto electrospun nanofiber membranes coated with polyaniline. Their results showed that polyaniline-coated membranes had a maximum adsorption capacity of 135 mg g^{-1} for PLLA/PANI membranes and 140 mg g^{-1} for PAN/PANI membranes [77]. Huong et al. found that the P-COOH-BSA nanofibrous membrane has a high and increasing adsorption capacity for TBO dye with rising initial dye concentrations. At concentrations of 2, 3, and 5 g L^{-1}, the adsorption capacities were 221.56 mg g^{-1}, 308.64 mg g^{-1}, and 357.14 mg g^{-1} respectively. The study also determined the pseudo-second-order constant for TBO dye adsorption, indicating that the model is appropriate for describing the adsorption process. However, they highlighted potential drawbacks of the membrane, such as high initial costs, the need for regular maintenance, and selective dye removal efficiency [75].

In the case of the study on the removal of CR dye using MNFs, the results shown in Table 2 demonstrate a positive correlation between the increase in MNFs mass and the enhancement of adsorption capacity as presented in Fig. 13.

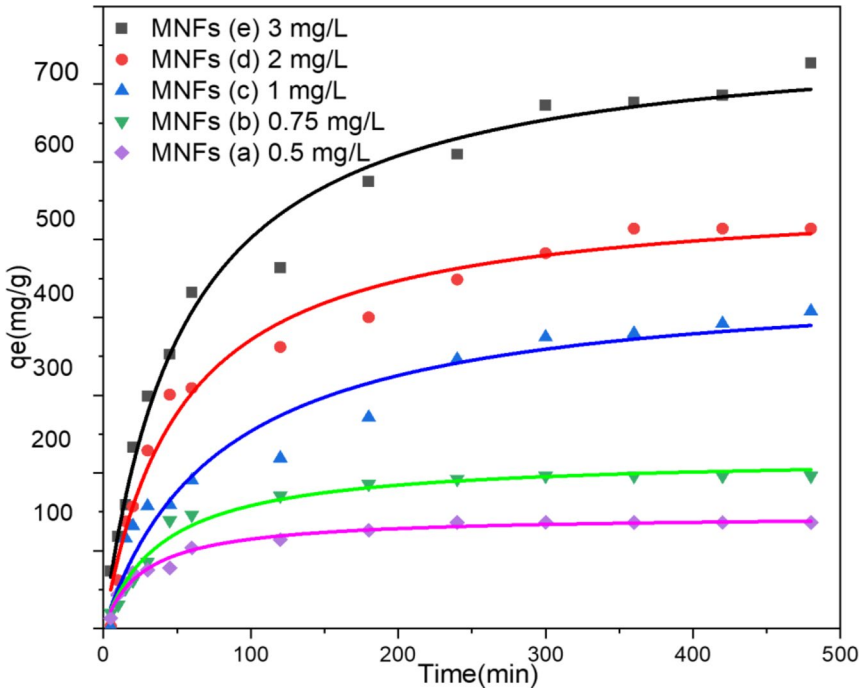

Fig. 13 Adsorption dynamics of CR using MNFs at different adsorbent concentrations

Table 3 Comparative evaluation of the Adsorption capacities of nanofibers

Nanofibers materials	Colour	Adsorption Rate (%)	Adsorption capacities (mg g^{-1})	References
P-COOH-BSA	Toluidine Blue	69	228	[58]
PLLA/CS-GO/TiO_2	Congo Red	74	260	[64]
PLLA/PANI	methylene blue	64	140	[66]
polymeric nanofibers	methylene blue	66	180	[57]
Fe^0/polyaniline	Congo Red	72	240	[61]

At a concentration of 0.5 g L^{-1} (MNFs(a)), the recorded adsorption capacity is 100 mg g^{-1}. This capacity increases to 150 mg g^{-1} when the MNFs concentration is raised to 0.75 g L^{-1} (MNFs(b)). A significant jump is observed at 1 g L^{-1} (MNFs(c)), where the adsorption capacity reaches 350 mg g^{-1}. At an even higher concentration of 2 g L^{-1} (MNFs(d)), the capacity rises to 480 mg g^{-1}. The highest level of efficiency is achieved at a concentration of 3 g L^{-1} (MNFs(e)), with an adsorption capacity peaking at 680 mg g^{-1}, indicating almost total saturation of the adsorption sites. These findings highlight the importance of the quantity of MNFs in optimizing the efficiency of adsorption in wastewater treatment systems.

Regarding the rate constant, it initially stands at 0.001 g mg^{-1} min^{-1} for MNFs(a) at 0.5 g L^{-1}, suggesting limited interaction between the dye and the adsorptive sites of MNFs. This constant increases to 0.016 g mg^{-1} min^{-1} for MNFs(b) at 0.75 g L^{-1}, indicating improved adsorption efficiency. For MNFs(c) at 1 g L^{-1}, the rate constant reaches 0.020 g mg^{-1} min^{-1}, revealing an increased availability of active sites. At a concentration of 2 g L^{-1} (MNFs(d)), the rate constant rises to 0.035 g mg^{-1} min^{-1}, confirming that higher masses lead to faster and more comprehensive adsorption. Finally, for MNFs(e) at 3 g L^{-1}, the peak rate constant is 0.050 g mg^{-1} min^{-1}, signaling near-complete saturation of adsorption sites. The study thus underscores the remarkable potential of MNFs in polluted water treatment, with rate constants significantly increasing in relation to the mass of MNFs.

Bhaumik et al. [79] have established that PPy-PANI NFs have a peak adsorption capability for Congo Red of 222.22 mg g^{-1} at 25 °C, achieving equilibrium in 30 to 120 min for the examined concentrations. The pseudo-second-order constant, k_2, ranges from 0.012 to 0.042 g/mg/min. In contrast, Zhang et al. [73] observed that NH2-ASEP nanofibers can adsorb up to 522 mg g^{-1} of the same dye at pH 8.0 and 25 °C, with a rate constant (k2) of 0.0012 g mg^{-1} min^{-1}. On the other hand, Habibi et al. [80] found carbon nanofibers to be effective for the dye's removal in water, boasting a maximum capacity of 265.2 mg g^{-1}. These fibers were produced via electrospinning and combined with $ZnFe_2O_4$: 1 wt% Ce^{3+} to create a composite. Their study also endorsed the pseudo-second-order kinetic model for its accuracy in describing the adsorption behavior on carbon nanofibers. Different previous results related to the Adsorption Capacities and rates of Nanofibers are shown in Table 3.

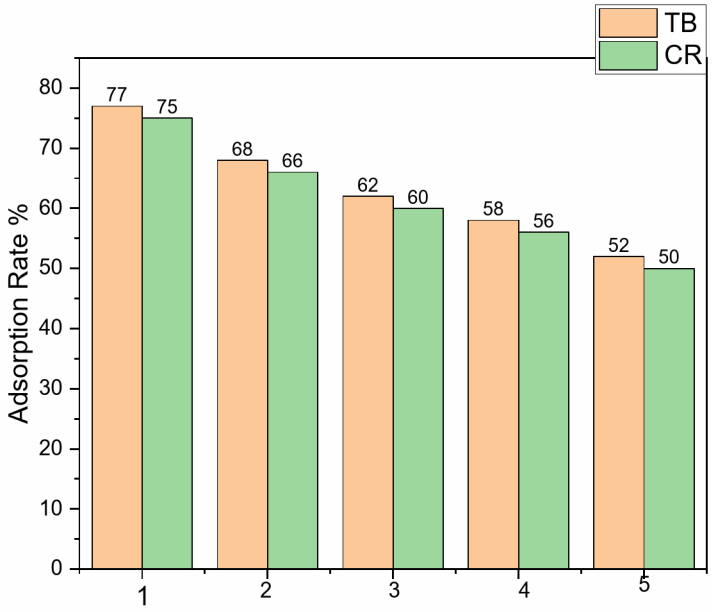

Fig. 14 Evaluation of the adsorption rate of magnetite nanofibers during cycles 5

It is evident that the adsorption rates and capacities of the composite nanofibers developed in this study outperform those reported in previous works. Specifically, the adsorption rates reached 78% for Toluidine Blue (TB) and 79% for Congo Red (CR) at a concentration of 1 g L^{-1}. The corresponding adsorption capacities were remarkably high, achieving 325 mg g^{-1} for TB and 350 mg g^{-1} for CR. These superior performance metrics highlight the efficiency of the composite nanofibers in dye removal applications. Moreover, the results underline the potential scalability of this approach for industrial wastewater treatment, particularly in addressing dye pollution. The performance could be further optimized by integrating the process with magnetic fields, enhancing both separation efficiency and operational feasibility in large-scale applications [45, 46, 81].

4.5 Regeneration Efficiency

The results (Fig. 14) show that magnetite nanofibers (MNF) exhibit good recyclability and significant regeneration potential for the adsorption of Congo Red (CR) and Toluidine Blue (TB) dyes. However, a progressive decrease in adsorption efficiency was observed over successive regeneration cycles. For Toluidine Blue, the adsorption capacity after the first regeneration was 77%, indicating that the MNFs retained a significant portion of their initial performance. After five cycles, this capacity decreased to 52%, reflecting a 25% loss in efficiency compared to the first cycle. A similar trend was observed for Congo Red, with an adsorption capacity of 75% after the first regeneration, dropping to 50% after five cycles, also indicating a 25% loss. This gradual decrease in performance can be attributed to the accumulation of residues on the MNFs' surface, structural changes, or partial saturation of active adsorption sites over multiple cycles. Other contributing factors might include oxidation or partial dissolution of the magnetite nanofibers during the regeneration processes. Despite this, the MNFs maintained over 50% of their adsorption capacity after five cycles, making them reusable for multiple practical applications. The differences in regeneration efficiency between the two dyes may be related to their specific properties, such as molecular size, chemical interactions with the MNF surface, or affinity for active sites. These results highlight that MNFs have good regeneration potential, although optimizing regeneration conditions (pH, regeneration agents, and temperature) could further improve their recyclability and extend their operational lifespan. In conclusion, MNFs prove to be promising materials for treating wastewater contaminated by dyes, maintaining acceptable efficiency even after several reuse cycles.

The novelty of this work lies in the development of a composite material that combines magnetite nanoparticles (MNPs) with nanofibers (MNFs) using the electrospinning technique. This innovative design integrates the high adsorption efficiency of MNPs with the enhanced structural stability, surface area, and porosity provided by the

nanofibers, resulting in a superior adsorption performance. Specifically, the MNFs demonstrated a 15% increase in adsorption efficiency for Toluidine Blue and a 20% increase for Congo Red compared to MNPs alone. Furthermore, the composite material exhibits versatility by effectively adsorbing both cationic and anionic dyes, making it suitable for a wide range of industrial wastewater applications. This study also provides detailed structural and kinetic analyses, offering insights into the mechanisms behind the improved performance, and establishes MNFs as a promising and environmentally friendly solution for dye removal.

5 Conclusion

This study highlights the innovative use of electrospinning to produce composite fibers combining inorganic MNPs with organic polymeric matrix, in order to produce improved adsorbents for ionic pollutants. Electrospinning, a versatile and efficient process, transforms magnetite nanoparticles into nanofibers with enhanced structure and surface area, thus facilitating improved dye adsorption. The elaborated MNFs demonstrating their superiority over traditional nanoparticles in ionic organic dyes with opposite charges, cationic toluidine blue and anionic Congo red, revealing exceptional elimination rates of 78% for toluidine blue at 1 g L^{-1} and 79% for Congo red at 1 g L^{-1} combined with impressive adsorption capacities of 325 mg g^{-1} and 350 mg g^{-1} respectively at 1 g L^{-1}. The efficiency of the process is highlighted by the good agreement of the adsorption kinetics with the pseudo-second-order kinetic model. An optimal balance between adsorption efficiency and rate, as well as the charge of the treated dyes, is required to design the appropriate electrospun using the studied MNFs.

Therefore, this study not only underscores the advantages of electrospinning as a synthesis method but also the potential of magnetite nanofibers as an advanced material for the ecological and economical treatment of industrial wastewater, offering an effective and sustainable solution for water decontamination.

The observed kinetics of adsorption demonstrate a strong correlation with the pseudo-second order kinetic model, highlighting the efficiency of the process. In this study, it was found that the adsorption capacity of the investigated MNFs is significantly higher for RC compared to TB. However, the adsorption rate of TB on MNFs was slightly higher than that of CR. Interestingly, although TB exhibits a slightly higher adsorption rate on MNFs compared to CR, the overall capacity remaining superior. This underscores the importance of carefully selecting parameters such as adsorption capacity, adsorption rate, and dye charge when designing electrospun membranes for removal of dyes from water bodies, thus mitigating environmental impact.

Furthermore, these results suggest significant potential for MNFs in real-world wastewater treatment systems, including industrial effluent remediation and environmental decontamination. Their high adsorption capacity, coupled with ease of synthesis and adaptability, positions MNFs as promising candidates for ecological and economical water purification solutions. However, certain challenges remain, such as optimizing large-scale production, ensuring long-term stability, and evaluating their performance in complex water matrices containing multiple contaminants as well as exploring the involved mechanisms in dyes elimination process.

Acknowledgements We would like to express our sincere gratitude to Prof. Gerardo F. Goya from the Instituto de Nanociencia y Materiales de Aragón (INMA), CSIC-Universidad de Zaragoza, Campus Río Ebro, 50018 Zaragoza, Spain, for providing to the doctorant Hajer Tlili the opportunity to produce nanofiber and experimental measurements. J.A.F.-G. acknowledged the Agencia Estatal de Investigación (AEI, Spain) for partial financial support. The tunisian team acknowledged The Ministry of Higher Education and Scientific Research of Tunisia for their continuous encouragement by project of young Research.

Author Contributions Conceptualization: Hajer Tlili, Anis Elaoud, Jesús Antonio Fuentes García, Mounir FerhiMagnetite nanoparticle synthesis and characterization: Hajer Tlili, Nedra Asses, Anis Elaoud, Mounir FerhiNanofibers preparation and characterization: Hajer Tlili, Jesús Antonio Fuentes García Investigation and analytic measurement: Hajer Tlili, Jesús Antonio Fuentes García Validation: Anis Elaoud, Jesús Antonio Fuentes García, Mounir Ferhi, Developed the theoretical formalism, performed the analytic calculations and numerical simulations: Hajer Tlili, Jesús Antonio Fuentes García.Writing—original draft preparation: Hajer Tlili, Anis Elaoud, Jesús Antonio Fuentes García, Nedra Asses, Karima Horchani-Naifer, Mounir FerhiReview and editing: Anis Elaoud, Jesús Antonio Fuentes García, Nedra Asses, Karima Horchani-Naifer, Mounir FerhiSupervision and coordination responsibility: Mounir FerhiAdministration and management for the research activity: Karima Horchani-NaiferAll authors have read and agreed to publish the revised version of the manuscript.

Funding No funding was received for conducting this study.

Data Availability No datasets were generated or analysed during the current study.

Declarations

Conflict of interest The authors declare that they have no known competing financial interests or personal relationships that could have appeared to influence the work reported in this paper.

References

1. Y. Wang, J. Zhu, G. Dong, Y. Zhang, N. Guo, J. Liu, Sulfonated halloysite nanotubes/polyethersulfone nanocomposite membrane

for efficient dye purification. Sep. Purif. Technol. **150**, 243–251 (2015). https://doi.org/10.1016/j.seppur.2015.07.005
2. A. Tkaczyk, K. Mitrowska, A. Posyniak, Synthetic organic dyes as contaminants of the aquatic environment and their implications for ecosystems: a review. Sci. Total Environ. **717**, 137222 (2020). https://doi.org/10.1016/j.scitotenv.2020.137222
3. F. Harrelkas, A. Azizi, A. Yaacoubi, A. Benhammou, M.N. Pons, Treatment of textile dye effluents using coagulation-flocculation coupled with membrane processes or adsorption on powdered activated carbon. Desalination. **235**, 330–339 (2009). https://doi.org/10.1016/j.desal.2008.02.012
4. S. Varjani, P. Rakholiya, H.Y. Ng, S. You, J.A. Teixeira, Microbial degradation of dyes: an overview. Bioresour Technol. **314**, 123728 (2020). https://doi.org/10.1016/j.biortech.2020.123728
5. A. Rehorek, M. Tauber, G. Gübitz, Application of power ultrasound for azo dye degradation. Ultrason. Sonochem. **11**, 177–182 (2004). https://doi.org/10.1016/j.ultsonch.2004.01.030
6. D. Ayodhya, G. Veerabhadram, A review on recent advances in photodegradation of dyes using doped and heterojunction based semiconductor metal sulfide nanostructures for environmental protection. Mater. Today Energy. **9**, 83–113 (2018). https://doi.org/10.1016/j.mtener.2018.05.007
7. J.H. Mo, Y.H. Lee, J. Kim, J.Y. Jeong, J. Jegal, Treatment of dye aqueous solutions using nanofiltration polyamide composite membranes for the dye wastewater reuse. Dyes Pigm. **76**, 429–434 (2008). https://doi.org/10.1016/j.dyepig.2006.09.007
8. A. Kausar, M. Iqbal, A. Javed, K. Aftab, Z. i., H. Nazli, H.N. Bhatti, S. Nouren, Dyes adsorption using clay and modified clay: a review. J. Mol. Liq. **256**, 395–407 (2018). https://doi.org/10.1016/j.molliq.2018.02.034
9. M.A.M. Salleh, D.K. Mahmoud, W.A.W.A. Karim, A. Idris, Cationic and anionic dye adsorption by agricultural solid wastes: a comprehensive review. Desalination. **280**, 1–13 (2011). https://doi.org/10.1016/j.desal.2011.07.019
10. M.T. Yagub, T.K. Sen, S. Afroze, H.M. Ang, Dye and its removal from aqueous solution by adsorption: a review. Adv. Colloid Interface Sci. **209**, 172–184 (2014). https://doi.org/10.1016/j.cis.2014.04.002
11. K. Sun, Z.H. Li, Preparations, properties and applications of chitosan based nanofibers fabricated by electrospinning. Express Polym. Lett. **5**, 342–361 (2011). https://doi.org/10.3144/expresspolymlett.2011.34
12. E. Selmer-Olsen, H.C. Ratnaweera, R. Pehrson, A novel treatment process for dairy wastewater with Chitosan produced shrimp-shell waste. Water Sci. Technol. **34**, 33–40 (1996). https://doi.org/10.1016/S0273-1223(96)00818-9
13. M.A. Rauf, S.M. Qadri, S. Ashraf, K.M. Al-Mansoori, Adsorption studies of Toluidine Blue from aqueous solutions onto gypsum. Chem. Eng. J. **150**, 90–95 (2009). https://doi.org/10.1016/j.cej.2008.12.008
14. S.K. Alpat, Ö. Özbayrak, Ş. Alpat, H. Akçay, The adsorption kinetics and removal of cationic dye, Toluidine Blue O, from aqueous solution with Turkish zeolite. J. Hazard. Mater. **151**, 213–220 (2008). https://doi.org/10.1016/j.jhazmat.2007.05.071
15. Y. Jiang, J.L. Gong, G.M. Zeng, X.M. Ou, Y.N. Chang, C.H. Deng, J. Zhang, H.Y. Liu, S.Y. Huang, Magnetic chitosan-graphene oxide composite for anti-microbial and dye removal applications. Int. J. Biol. Macromol. **82**, 702–710 (2016). https://doi.org/10.1016/j.ijbiomac.2015.11.021
16. C. Jiang, X. Wang, D. Qin, W. Da, B. Hou, C. Hao, J. Wu, Construction of magnetic lignin-based adsorbent and its adsorption properties for dyes. J. Hazard. Mater. **369**, 50–61 (2019). https://doi.org/10.1016/j.jhazmat.2019.02.021
17. C. Li, T. Lou, X. Yan, Y. ze Long, G. Cui, X. Wang, Fabrication of pure chitosan nanofibrous membranes as effective absorbent for dye removal. Int. J. Biol. Macromol. **106**, 768–774 (2018). https://doi.org/10.1016/j.ijbiomac.2017.08.072
18. M.G. Yazdi, M. Ivanic, A. Mohamed, A. Uheida, Surface modified composite nanofibers for the removal of indigo carmine dye from polluted water. RSC Adv. **8**, 24588–24598 (2018). https://doi.org/10.1039/c8ra02463d
19. A. Akbari, F.J. Sheshdeh, V. Jabbari, Novel nanofiberous membrane fabricated via electrospinning of wastage fuzzes of mechanized carpet used for dye removal of the carpet dyeing wastewater. J. Environ. Sci. Health Tox Hazard. Subst. Environ. Eng. **47**, 847–853 (2012). https://doi.org/10.1080/10934529.2012.664999
20. Q. Wang, D. Gao, C. Gao, Q. Wei, Y. Cai, J. Xu, X. Liu, Y. Xu, Removal of a cationic dye by adsorption/photodegradation using electrospun PAN/O-MMT composite nanofibrous membranes coated with TiO2. Int. J. Photoenergy. **2012** (2012). https://doi.org/10.1155/2012/680419
21. S. Swaminathan, A. Muthumanickkam, N.M. Imayathamizhan, An effective removal of methylene blue dye using polyacrylonitrile yarn waste/graphene oxide nanofibrous composite. Int. J. Environ. Sci. Technol. **12**, 3499–3508 (2015). https://doi.org/10.1007/s13762-014-0711-z
22. J.A. Flood-Garibay, M.A. Méndez-Rojas, Synthesis and characterization of magnetic wrinkled mesoporous silica nanocomposites containing Fe3O4 or CoFe2O4 nanoparticles for potential biomedical applications. Colloids Surf. Physicochem Eng. Asp. **615** (2021). https://doi.org/10.1016/j.colsurfa.2021.126236
23. L.S. Wan, Z.K. Xu, H.L. Jiang, Fibrous membranes electrospinning from acrylonitrue-based polymers: specific absorption behaviors and states of water. Macromol. Biosci. **6**, 364–372 (2006). https://doi.org/10.1002/mabi.200600017
24. H. Wang, L. Kong, G.R. Ziegler, Aligned wet-electrospun starch fiber mats. Food Hydrocoll. **90**, 113–111 (2019). https://doi.org/10.1016/j.foodhyd.2018.12.008
25. B.Y. Yu, P.Y. Chen, Y.M. Sun, Y.T. Lee, T.H. Young, The behaviors of human mesenchymal stem cells on the poly(3-hydroxybutyrate-co-3-hydroxyhexanoate) (PHBHHx) membranes. Desalination. **234**, 204–211 (2008). https://doi.org/10.1016/j.desal.2007.09.087
26. T. Subbiah, G.S. Bhat, R.W. Tock, S. Parameswaran, S.S. Ramkumar, Electrospinning of nanofibers. J. Appl. Polym. Sci. **96**, 557–569 (2005). https://doi.org/10.1002/app.21481
27. D. Fallahi, M. Rafizadeh, N. Mohammadi, B. Vahidi, Effect of LiCl and non-ionic surfactant on morphology of polystyrene electrospun nanofibers. E-Polymers. 1–10 (2008). https://doi.org/10.1515/epoly.2008.8.1.644
28. M. Rafizadeh, D. Fallahi, N. Mohammadi, B. Vahidi, Effects of feed rate and solution conductivity on jet current and fiber diameter in electrospinning of polyacrylonitrile solutions. E-Polymers. 1–8 (2009). https://doi.org/10.1515/epoly.2009.9.1.1250
29. J.A. Naser, T.A. Himdan, A.J. Ibraheim, Adsorption kinetic of malachite green dye from aqueous solutions by electrospun nanofiber mat. Orient. J. Chem. **33**, 3121–3129 (2017). https://doi.org/10.13005/ojc/330654
30. F.E. Ahmed, B.S. Lalia, R. Hashaikeh, A review on electrospinning for membrane fabrication: challenges and applications. Desalination. **356**, 15–30 (2015). https://doi.org/10.1016/j.desal.2014.09.033
31. A. Mehdizadeh, P. Najafi Moghadam, S. Ehsanimehr, A.R. Fareghi, Preparation of a new magnetic nanocomposite for the removal of dye pollutions from aqueous solutions: synthesis and characterization. Mater. Chem. Horiz. **1**(1), 23–34 (2022)
32. H.E. Reynel-Ávila, K.I. Camacho-Aguilar, A. Bonilla-Petriciolet, D.I. Mendoza-Castillo, H.A. González-Ponce, R. Trejo-Valencia, Engineered magnetic carbon-based adsorbents for the removal

of water priority pollutants: an overview. Adsorp. Sci. Technol. (2021). https://doi.org/10.1155/2021/9917444
33. A.M. Nasir et al., Recent progress on fabrication and application of electrospun nanofibrous photocatalytic membranes for wastewater treatment: a review. J. Water Process Eng. **40**(2020), 101878 (2021). https://doi.org/10.1016/j.jwpe.2020.101878
34. U. H.N. Kamran, S. Bhatti, Noreen, M.A. Tahir, Chemically modified sugarcane bagasse-based biocomposites for efficient removal of acid red 1 dye: kinetics, isotherms, thermodynamics, and desorption studies. Chemosphere (2022). https://doi.org/10.1016/j.chemosphere.2021.132796
35. U. Park, Hybrid biochar supported transition metal doped MnO_2 composites: efficient contenders for lithium adsorption and recovery from aqueous solutions. Desalination (2022). https://doi.org/10.1016/j.desal.2021.115387
36. U. Kamran, S.Y. Lee, K.Y. Rhee, S.J. Park, Rice husk valorization into sustainable Ni@TiO_2/biochar nanocomposite for highly selective Pb(II) ions removal from an aqueous media. Chemosphere (2023). https://doi.org/10.1016/j.chemosphere.2023.138210
37. A.U.K. Baig, H. Jamal, M.U. Arif, M. Hassan, New $Y_{0.045}$ $Ni_{0.045}$ $Fe_{2.91}$ O_4 nanowires decorated over mesoporous silica for crystal violet removal: response surface methodology optimization, kinetics, and isothermal studies. Ceram. Int. https://doi.org/10.1016/j.ceramint.2024.02.177
38. N.U. Ali, B. Adalat, Methylene blue adsorption using boric acid functionalized activated carbon: kinetics, isothermal, and thermodynamic studies. Chem. Eng. Technol. (2024). https://doi.org/10.1002/ceat.202400016
39. M.U. Saeed, A. Kamran, M.I. Khan, Jamal, *Mangifera indica* stone-assisted layered double hydroxide biocomposites: efficient contenders for reactive dye adsorption from aqueous sources. New. J. Chem. (2024). https://doi.org/10.1039/D3NJ04133F
40. Z. Arshad et al., Comparison of electrospun titania and zinc oxide nanofibers for perovskite solar cells and photocatalytic degradation of methyl orange dye. Catalysts (2023). https://doi.org/10.3390/catal13071062
41. Z. Arshad et al., Enhanced charge transport characteristics in zinc oxide nanofibers via Mg^{2+} doping for electron transport layer in perovskite solar cells and antibacterial textiles. Ceram. Int. **48**, 24363–24371 (2022). https://doi.org/10.1016/j.ceramint.2022.05.018
42. W. Zhang, Z. He, Y. Han, Q. Jiang, C. Zhan, K. Zhang, Z. Li, R. Zhang, Structural design and environmental applications of electrospun nanofibers. Compos. Part. Appl. Sci. Manuf. **137**, 106009 (2020). https://doi.org/10.1016/j.compositesa.2020.106009
43. M. Najafi, M.W. Frey, Electrospun nanofibers for chemical separation. Nanomaterials (2020). https://doi.org/10.3390/nano10050982
44. O.K. Pereao, C. Bode-Aluko, G. Ndayambaje, O. Fatoba, L.F. Petrik, Electrospinning: polymer nanofibre adsorbent applications for metal ion removal. J. Polym. Environ. **25**, 1175–1189 (2017). https://doi.org/10.1007/s10924-016-0896-y
45. H. Tlili, A. Elaoud, N. Asses, K. Horchani-Naifer, M. Ferhi, G.F. Goya, J.A. Fuentes-García, Reduction of oxidizable pollutants in waste water from the Wadi El Bey river basin using magnetic nanoparticles as removal agents. Magnetochemistry (2023). https://doi.org/10.3390/MAGNETOCHEMISTRY9060157
46. J.A. Fuentes-García, B. Sanz, R. Mallada, M.R. Ibarra, G.F. Goya, Magnetic nanofibers for remotely triggered catalytic activity applied to the degradation of organic pollutants. Mater. Des. **226**, 111615 (2023). https://doi.org/10.1016/J.MATDES.2023.111615
47. D.J. Förster, D. Anh, V. Onuseit, R. Weber, T. Graf, in *Lasers in Manufacturing Conference 2015 Energy Transfer Mechanisms During Laser Pulsed Processing of Metals* (2015)
48. P.G. Coelho, P. Sudack, M. Suzuki, K.S. Kurtz, G.E. Romanos, N.R.F.A. Silva, In vitro evaluation of the implant abutment connection sealing capability of different implant systems. J. Oral Rehabil. **35**, 917–924 (2008). https://doi.org/10.1111/j.1365-2842.2008.01886.x
49. J. Wang, X. Guo, Adsorption kinetic models: Physical meanings, applications, and solving methods. J. Hazard. Mater. **390**, 122156 (2020). https://doi.org/10.1016/j.jhazmat.2020.122156
50. X. Guo, J. Wang, A general kinetic model for adsorption: theoretical analysis and modeling. J. Mol. Liq. **288**, 111100 (2019). https://doi.org/10.1016/j.molliq.2019.111100
51. E.D. Revellame, D.L. Fortela, W. Sharp, R. Hernandez, M.E. Zappi, Adsorption kinetic modeling using pseudo-first order and pseudo-second order rate laws: a review. Clean. Eng. Technol. **1**, 100032 (2020). https://doi.org/10.1016/j.clet.2020.100032
52. Y. Ho, G. McKay, Sorption of dye from aqueous solution by peat. Chem. Eng. J. **70**, 115–124 (1998). https://doi.org/10.1016/S1385-8947(98)00076-X
53. Y. Ho, A.E. Ofomaja, Pseudo-second-order model for lead ion sorption from aqueous solutions onto palm kernel fiber. J. Hazard. Mater. **129**, 137–142 (2006). https://doi.org/10.1016/j.jhazmat.2005.08.020
54. S. Brunauer, P.H. Emmett, E. Teller, Adsorption of gases in multimolecular layers. J. Am. Chem. Soc. **60**, 309–319 (1938). https://doi.org/10.1021/ja01269a023
55. L. Largitte, R. Pasquier, A review of the kinetics adsorption models and their application to the adsorption of lead by an activated carbon. Chem. Eng. Res. Des. **109**, 495–504 (2016). https://doi.org/10.1016/j.cherd.2016.02.006
56. S.P.D. Monte Blanco, F.B. Scheufele, A.N. Módenes, F.R. Espinoza-Quiñones, P. Marin, A.D. Kroumov, C.E. Borba, Kinetic, equilibrium and thermodynamic phenomenological modeling of reactive dye adsorption onto polymeric adsorbent. Chem. Eng. J. **307**, 466–475 (2017). https://doi.org/10.1016/j.cej.2016.08.104
57. Y. Hu, X. Guo, C. Chen, J. Wang, Algal sorbent derived from *Sargassum horneri* for adsorption of cesium and strontium ions: equilibrium, kinetics, and mass transfer. Appl. Microbiol. Biotechnol. **103**, 2833–2843 (2019). https://doi.org/10.1007/s00253-019-09619-z
58. X. Guo, J. Wang, Sorption of antibiotics onto aged microplastics in freshwater and seawater. Mar. Pollut. Bull. **149**, 110511 (2019). https://doi.org/10.1016/j.marpolbul.2019.110511
59. Y. Liu, L. Shen, From Langmuir kinetics to first- and second-order rate equations for adsorption. Langmuir. **24**, 11625–11630 (2008). https://doi.org/10.1021/la801839b
60. S. Azizian, Kinetic models of sorption: a theoretical analysis. J. Colloid Interface Sci. **276**, 47–52 (2004). https://doi.org/10.1016/j.jcis.2004.03.048
61. Y.S. Ho, Review of second-order models for adsorption systems. J. Hazard. Mater. **136**, 681–689 (2006). https://doi.org/10.1016/j.jhazmat.2005.12.043
62. R. Ezzati, Derivation of pseudo-first-order, pseudo-second-order and modified pseudo-first-order rate equations from Langmuir and Freundlich isotherms for adsorption. Chem. Eng. J. **392**, 123705 (2020). https://doi.org/10.1016/j.cej.2019.123705
63. C.S. Zhu, L.P. Wang, W. bin Chen, Removal of Cu(II) from aqueous solution by agricultural by-product: peanut hull. J. Hazard. Mater. **168**, 739–746 (2009). https://doi.org/10.1016/j.jhazmat.2009.02.085
64. A. Ritter, R. Muñoz-Carpena, Performance evaluation of hydrological models: statistical significance for reducing subjectivity in goodness-of-fit assessments. J. Hydrol. (Amst). **480**, 33–45 (2013). https://doi.org/10.1016/J.JHYDROL.2012.12.004
65. S. Venkateswarlu, B. Natesh Kumar, C.H. Prasad, P. Venkateswarlu, N.V.V. Jyothi, Bio-inspired green synthesis of Fe_3O_4 spherical magnetic nanoparticles using *Syzygium cumini* seed extract. Phys. B Condens. Matter. **449**, 67–71 (2014). https://doi.org/10.1016/j.physb.2014.04.031

66. M. Morel, F. Martínez, E. Mosquera, Synthesis and characterization of magnetite nanoparticles from mineral magnetite. J. Magn. Magn. Mater. **343**, 76–81 (2013). https://doi.org/10.1016/j.jmmm.2013.04.075
67. L. Wang, Y. Li, P. Han, Electrospinning preparation of gC_3N_4/Nb_2O_5 nanofibers heterojunction for enhanced photocatalytic degradation of organic pollutants in water. Sci. Rep. **11**(1), 1–12 (2021). https://doi.org/10.1038/s41598-021-02161-x
68. N. Li, W. Wang, L. Zhu, W. Cui, X. Chen, B. Zhang, Z. Zhang, A novel electro-cleanable PAN-ZnO nanofiber membrane with superior water flux and electrocatalytic properties for organic pollutant degradation. Chem. Eng. J. **421**, 127857 (2021). https://doi.org/10.1016/j.cej.2020.127857
69. D.T.M. Huong, W.S. Chai, P.L. Show, Y.L. Lin, C.Y. Chiu, S.L. Tsai, Y.K. Chang, Removal of cationic dye waste by nanofiber membrane immobilized with waste proteins. Int. J. Biol. Macromol. **164**, 3873–3884 (2020). https://doi.org/10.1016/j.ijbiomac.2020.09.020
70. N. Nady, M.H. Abdel Rehim, A.A. Badawy, Dye removal membrane from electrospun nanofibers of blended polybutylenesuccinate and sulphonated expanded polystyrene waste. Sci. Rep. **13**, 1–12 (2023). https://doi.org/10.1038/s41598-023-42424-3
71. W. Yang, S.S. Zare, Bio-originated mesosilicate SBA-15: synthesis, characterization, and application for heavy metal removal. J. Nat. Water. (2024). https://doi.org/10.1038/s41545-024-00340-7
72. R. Das, M. Bhaumik, S. Giri, A. Maity, Sonocatalytic rapid degradation of Congo red dye from aqueous solution using magnetic FeO/polyaniline nanofibers. Ultrason. Sonochem. **37**, 600–613 (2017). https://doi.org/10.1016/j.ultsonch.2017.02.022
73. M. Abid, S. Sayegh, I. Iatsunskyi, E. Coy, G. Lesage, A. Ramanavicius, A. Ben Haj Amara, M. Bechelany,, Design of halloysite-based nanocomposites by electrospinning for water treatment. Colloids Surf. Physicochem Eng. Asp. **651**, 129696 (2022). https://doi.org/10.1016/j.colsurfa.2022.129696
74. H.O. Alsaab, S. Shirazian, N. Pirestani, R. Soltani, Sustainable synthesis and dual adsorption of methyl orange and cadmium ions using biogenic silica-based fibrous silica functionalized with crown ether ionic liquid. J. Colloid Interface Sci. (2025). https://doi.org/10.1016/j.jcis.2024.10.103
75. S. Shirazian, T. Huynh, N. Pirestani, R. Soltani, A. Marjani, B. Albadarin, Sarkar efficient green Cr(VI) adsorbent from sorghum waste: eco-designed functionalized mesoporous silica FDU-12. J. Colloid Interface Sci. (2024). https://doi.org/10.1016/j.jcis.2024.03.030
76. S.Shirazian, S. Alshehri, A.H. Almalki, R.M. Alzhrani, N. Pirestani and R. Soltani, Eco-friendly synthesis of crown-ether functionalized silica nanospheres from sorghum waste for thallium adsorption. J. Taiwan Inst. Chem. Eng. (2025). https://doi.org/10.1016/j.jtice.2024.105851
77. N. Mohammad, Y. Atassi, Adsorption of methylene blue onto electrospun nanofibrous membranes of polylactic acid and polyacrylonitrile coated with chloride doped polyaniline. Sci. Rep. **10**, 1–19 (2020). https://doi.org/10.1038/s41598-020-69825-y
78. M. Bhaumik, R. McCrindle, A. Maity, Efficient removal of Congo Red from aqueous solutions by adsorption onto interconnected polypyrrole-polyaniline nanofibres. Chem. Eng. J. **228**, 506–515 (2013). https://doi.org/10.1016/j.cej.2013.05.026
79. J. Zhang, Z. Yan, J. Ouyang, H. Yang, D. Chen, Highly dispersed sepiolite-based organic modified nanofibers for enhanced adsorption of Congo Red. Appl. Clay Sci. **157**, 76–85 (2018). https://doi.org/10.1016/j.clay.2018.02.031
80. M.K. Habibi, S.M. Rafiaei, A. Alhaji, M. Zare, Synthesis of $ZnFe_2O_4$: 1 wt% Ce^{3+}/carbon fibers composite and investigation of its adsorption characteristic to remove Congo red dye from aqueous solutions. J. Alloys Compd. **890**, 161901 (2022). https://doi.org/10.1016/j.jallcom.2021.161901
81. H. Tlili, A. Elaoud, N. Asses, K. Horchani-Naifer, M. Ferhi, New process for the treatment of polluted water using the coupling of nanoparticles (Fe_3O_4) and intense magnetic system. Emerg. Mater. (2023). https://doi.org/10.1007/S42247-023-00619-4/METRICS